Available online at www.sciencedirect.com
SCIENCE DIRECT®
Geochimica et Cosmochimica Acta 70 (2006) 306–322
Geochimica
www.elsevier.com/locate/gca

The effect of iron on montmorillonite stability. (I) Background and thermodynamic considerations

James Wilson [a,b,c,*], David Savage [d], Javier Cuadros [b], Masahiro Shibata [e], K.Vala Ragnarsdottir [c]

[a] Chemical Hazards and Poisons Division (London), Health Protection Agency, Medical Toxicology Unit, Avonley Road, London SE14 5ER, UK
[b] Department of Mineralogy, The Natural History Museum, Cromwell Road, London SW7 5BD, UK
[c] Department of Earth Sciences, University of Bristol, Wills Memorial Building, Queen's Road, Clifton, Bristol BS8 1RJ, UK
[d] Quintessa Ltd., 24 Trevor Road, West Bridgford, Nottingham NG2 6FS, UK
[e] Japan Nuclear Cycle Development Institute (JNC), Tokaimura Prefecture, Japan

Received 8 November 2004; accepted in revised form 7 September 2005

Abstract

It is envisaged that high-level nuclear waste (HLW) will be disposed of in underground repositories. Many proposed repository designs include steel waste canisters and bentonite backfill. Natural analogues and experimental data indicate that the montmorillonite component of the backfill could react with steel corrosion products to produce non-swelling Fe-rich phyllosilicates such as chamosite, berthierine, or Fe-rich smectite. In K-bearing systems, the alteration of montmorillonite to illite/glauconite could also be envisaged. If montmorillonite were altered to non-swelling minerals, the swelling capacity and self-healing properties of the bentonite backfill could be reduced, thereby diminishing backfill performance. The main aim of this paper was to investigate Fe-rich phyllosilicate mineral stability at the canister–backfill interface using thermodynamic modelling. Estimates of thermodynamic properties were made for Fe-rich clay minerals in order to construct approximate phase-relations for end-member/simplified mineral compositions in logarithmic activity space. Logarithmic activity diagrams (for the system Al_2O_3–FeO–Fe_2O_3–MgO–Na_2O–SiO_2–H_2O) suggest that if pore waters are supersaturated with respect to magnetite in HLW repositories, Fe(II)-rich saponite is the most likely montmorillonite alteration product (if $f_{O_{2(g)}}$ values are significantly lower than magnetite–hematite equilibrium). Therefore, the alteration of montmorillonite may not be detrimental to nuclear waste repositories that include Fe, as long as the swelling behaviour of the Fe-rich smectite produced is maintained. If $f_{O_{2(g)}}$ exceeds magnetite–hematite equilibrium, and solutions are saturated with respect to magnetite in HLW repositories, berthierine is likely to be more stable than smectite minerals. The alteration of montmorillonite to berthierine could be detrimental to the performance of HLW repositories.
© 2006 Published by Elsevier Inc.

1. Introduction

1.1. High-level nuclear waste disposal

High-level nuclear waste (HLW) consists of either spent nuclear fuel or products generated from its reprocessing. It is envisaged that HLW will be disposed of in underground repositories (Apted, 1995), which typically include bentonite (or bentonite-sand) backfill emplaced around the metal canisters containing HLW (Fig. 1). Bentonite is a smectite-rich rock. In the case of nuclear waste disposal, the smectite component of bentonite is the Mg-bearing aluminous end-member, montmorillonite. Many proposed HLW–EBS designs (e.g., the Japanese and Swiss concepts) include steel containers. Bentonite barriers are favoured for repositories sited below the water table, primarily because they have the following properties: (1) low hydraulic conductivities (10^{-12} to 10^{-14} m s^{-1}, Bucher and Spiegel, 1984; Pusch, 1992); (2) "self-healing" behaviour (Pusch, 1992; Oscarson

* Corresponding author.
E-mail address: James.Wilson@HPA.org.uk (J. Wilson).

0016-7037/$ - see front matter © 2006 Published by Elsevier Inc.
doi:10.1016/j.gca.2005.10.003

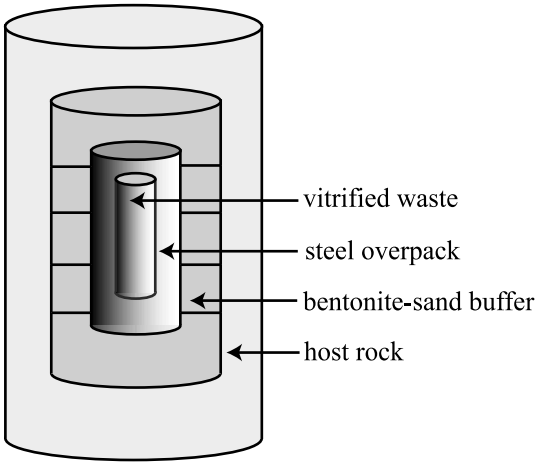

Fig. 1. Multiple-barrier HLW–EBS concept (JNC).

et al., 1996), and (3) high cation exchange and adsorption capacities. In order for bentonite barriers to perform their required functions, the smectite component must be stable over prolonged periods of time, possibly up to and greater than 10^6 years (Apted, 1995). The alteration of montmorillonite to non-swelling 1:1 or 2:1 phyllosilicates could result in the undesirable loss of swelling, self-healing and cation exchange capacities. In addition, further cation exchange and sorptive capacities could be reduced if smectite was altered to larger crystals as the adsorption site density on crystal edges would be decreased.

The alteration of montmorillonite (idealised here as $X^{z}_{0.35/z}Al_{1.65}Mg_{0.35}Si_4O_{10}(OH)_2 \cdot nH_2O$, where X is an interlayer cation of charge z) to trioctahedral Fe(II)-rich smectite (theoretical Fe end-member saponite idealised here as $X^{z}_{0.35/z}Fe_3Si_{3.65}Al_{0.35}O_{10}(OH)_2 \cdot nH_2O$) may also change the rheological properties of the backfill. Relatively few studies have been conducted on Fe(II)-rich smectite, due to its instability under ambient atmospheric conditions. However, Kohyama et al. (1973) report significant oxidation in less than an hour, resulting in a decrease of the smectite b-axis parameter with increasing Fe(III) content. Kohyama et al. (1973) suggest that the oxidation process involved consumption of structural OH and atmospheric oxygen. Badaut et al. (1985) also describe a similar Fe(II)-rich saponite which was seen to be unstable in air. Many investigations into the properties of Fe(III)-rich smectite have been conducted on nontronite (idealised here as $X^{z}_{0.35/z}Fe_2Si_{3.65}Al_{0.35}O_{10}(OH)_2 \cdot nH_2O$), or more aluminous "ferruginous smectite" after the reduction of structural Fe(III) to Fe(II) by the application of a reducing agent (generally Na-dithionite in a citrate–bicarbonate pH buffer, Stucki and Roth, 1977; Stucki et al., 1984, 1996; Stucki and Tessier, 1991). These studies show that the reduction of Fe(III) to Fe(II) in smectite may result in an increase in layer charge and ordering in the *hk* lattice planes. Furthermore, aqueous suspensions of ferruginous smectite have an increased viscosity subsequent to Fe reduction due to increased interparticle attraction. Several mechanisms by which reduction of Fe(III) to Fe(II) may occur (involving interactions between $OH_{(structural)}$, $H_2O_{(l)}$, and H^+) have been suggested (Stucki and Roth, 1977; Lear and Stucki, 1989; Drits and Manceau, 2000; Manceau et al., 2000b).

The experiments by Stucki et al. (1984, 1996); Stucki and Tessier (1991) imply that if the montmorillonite component of a HLW–EBS buffer material was replaced by high-charge Fe(II)-rich smectite mineral, the performance of the repository could be, to some extent, degraded due to attractive forces between smectite layers being greater than those associated with low to moderate charge aluminous smectite.

The stability of bentonite may be investigated by a consideration of natural analogues, by the construction of geochemical models and through hydrothermal experimentation. Previous discussions on the stability of bentonite in HLW repositories generally focus on the potential for the conversion of smectite to illite (Pusch, 1993; Grauer, 1994; Madsen, 1998; Meunier et al., 1998).

1.2. Natural analogues

In HLW repositories, two reaction pathways may be envisaged for an iron waste canister and a clay buffer/backfill: (1) the alteration of montmorillonite to Fe-rich smectite; and (2) the replacement of smectite to non-swelling phyllosilicates, such as chlorite. Fe-rich smectites (dioctahedral nontronite or Fe-rich, trioctahedral saponite), occur in a variety of geological settings usually where minerals in Fe-rich rocks have undergone alteration under aqueous or sub-aerial conditions. For example, Fe-rich smectite has been seen to precipitate in hot (56 °C) brines in the geothermal system of the Red Sea (Bischoff, 1972). Nontronite occurs in weathered iron-rich rocks such as basalts (e.g., Sherman et al., 1962) and Fe-rich saponites derived from the weathering of tuffs have also been described (Kohyama et al., 1973). Fe-rich 1:1 phyllosilicates (berthierine and odinite) are found in a variety of geological settings, including laterites, low-temperature sedimentary and low-grade metamorphic rocks and hydrothermal systems and are often associated with ironstones (e.g., Van Houten and Purucker, 1984; Siehl and Thein, 1989; Taylor, 1990; Toth and Fritz, 1997a,b). Several workers report the existence of 1:1 minerals that are interlayered with chlorite in diagenetic environments and hydrothermal systems (e.g., Hillier and Velde, 1992; Jiang et al., 1992; Ahn and Peacor, 1995). It has been suggested that berthierine may be a diagenetic precursor to chlorite, and that chlorite formation can occur in sandstones at a depth corresponding to a temperature of 90 °C (Aagaard et al., 2000). In addition, a wide range of Fe-rich K-bearing clays can occur in marine environments (Odin, 1988).

Chloritisation of smectite is seen in several geological settings, including the hydrothermal alteration of volcaniclastic rocks (e.g., Inoue and Utada, 1991), metamorphism of pelitic rocks (e.g., Jiang and Peacor, 1994), hydrothermal and regional metamorphism of Mg-silicates and glass in basic igneous rocks (Ragnarsdottir et al., 1984; Schiffman and Fridleiffson, 1991; Shau and Peacor, 1992; Robinson et al., 1993; Schiffman and Staudigel, 1995; Schmidt

and Robinson, 1997) and the hydrothermal alteration of mafic minerals in amphibolites and gneisses (Beaufort and Meunier, 1994). Chloritisation of smectite in late-stage diagenetic to early-stage metamorphic systems may involve the progressive conversion of trioctahedral smectite to chlorite (often via corrensite, Merriman and Peacor, 1999). The review of hydrothermally altered metabasites given by Robinson et al. (2002), indicates that in such systems smectite may be persistent up to a temperature of ~200 °C with alteration occurring at temperatures generally exceeding ~120 °C. After closure, HLW repositories are expected to experience initial temperature conditions that may exceed 100 °C due to the heat from HLW. Long-term ambient temperature conditions are expected to be less than 100 °C. Temperatures of 60 and 45 °C are envisaged for the Swiss and Japanese disposal concepts respectively (Grauer, 1994; JNC, 1999). The temperatures at which significant smectite chloritisation is observed may therefore be higher than those expected to occur over prolonged periods in a HLW repository.

Late-stage diagenetic to early-stage metamorphic systems do not provide unequivocal temperature–pressure conditions under which chlorite is likely to be stable in other systems such as engineered nuclear waste repositories, due to uncertainties associated with determining whether or not an observed phase assemblage represents equilibrium or metastable equilibrium conditions.

Existing studies of geological systems alone do not provide a clear indication of the expected evolution of phase assemblages in HLW repositories. Studies of co-existing mineral–fluid compositions for systems including Fe-rich clay minerals such as Fe(II)-bearing saponite are lacking.

1.3. Validity of the thermodynamic modelling of clay mineral–fluid interactions

The validity of thermodynamic models which include clay minerals has been debated in the literature, on the basis of the following (somewhat interrelated) hypotheses: (1) clay minerals do not comply with the phase rule and therefore should not be included in thermodynamic models; (2) clay minerals exist in a state of disequilibrium; and (3) thermodynamic models including clay minerals such as illite and smectite may not represent true equilibrium conditions and it has been argued that clay minerals are metastable with respect to phyllosilicates of greater homogeneity, such as those belonging to the talc–pyrophyllite and mica groups (Aja and Rosenberg, 1992, 1996; Essene and Peacor, 1995, 1997; Lippman, 1977, 1982; May et al., 1986). It is clear that thermodynamic models of mineral–fluid equilibria including smectite are subject to some uncertainty in terms of their validity and that kinetic constraints are partly responsible for the clay mineral assemblages observed in natural systems. However, it seems unlikely that solute activities have no influence on the type of mineral that forms in low-temperature systems, even if clay mineral assemblages are influenced by reaction kinetics. Hence our attempt in this communication at constructing simplified thermochemical models that include iron-rich clays.

1.4. Aims and objectives

The overall aim of this work was to determine the likely effect of iron on montmorillonite stability, which is especially relevant for maximising the safety of HLW repositories. Given the uncertainties associated with the thermodynamic modelling of clay mineral stability, the lack of measured thermodynamic data for iron-rich clays and the paucity of data on montmorillonite–iron interactions, the objectives of this paper and its companion paper (Wilson et al., 2006) are: (1) to generate estimates of standard molal thermodynamic properties of Fe-rich clay minerals; (2) to provide simplified thermodynamic modelling of Fe-rich clay mineral stability and to determine controls on dissolved Fe activities under low oxygen conditions; (3) to conduct experiments to determine whether the mineral alterations predicted by the models can be observed experimentally (thereby giving an indication of the validity of using estimated thermodynamic data in predicting mineral alteration pathways); and (4), to determine whether the kinetics of montmorillonite alteration to Fe-rich minerals are measurable under laboratory conditions.

The issues surrounding the validity of thermodynamic modelling of clay minerals, the use of simplified clay mineral compositions and the need to use estimated thermodynamic data for clays mean that the models included in this paper are not as quantitative as the authors would have wished. Given the many problems associated with thermodynamic modelling of clay minerals, the models provided in this paper, at best, give approximate zones of clay mineral stability in logarithmic activity space, which can be used to give a broad indication of the conditions that will promote the alteration of montmorillonite to either an Fe-rich 1:1 or 2:1 mineral structure. In addition to the models of clay mineral stability, reactions determining dissolved Fe activities are also considered in the scenario of a HLW repository, whereby steel containers are corroding to produce mixed valence iron oxides. Throughout the whole of the earth's crust, the solubilities of iron sulphides and carbonates would also exert influence Fe activities. However, it is beyond the scope of this work to fully consider all of these systems. The models generated in this paper are evaluated using experimental data in a companion paper presented by Wilson et al. (2006), whereby mixtures of native iron, magnetite, and montmorillonite are reacted with NaCl and $FeCl_2$ solutions under hydrothermal conditions.

2. Thermodynamic data

2.1. Mineral compositions and standard states

The thermodynamic models presented in this work include simplified compositions. The purpose of these models

is to show the regions of mineral (meta)stability in logarithmic activity space for Fe-rich phyllosilicate structures (both 1:1 and 2:1). Given the variability of clay mineral composition on a unit cell level (Essene and Peacor, 1995) and the interstratified nature of clay minerals (Środoń, 1999) the validity of treating smectites as solid solutions of stoichiometric phyllosilicates has been questioned (Aja and Rosenberg, 1992). Of the solid solution approaches available for smectite minerals, the homological site mixing model developed by Aagaard and Helgeson (1983) appears to be the most relevant. However, this approach is not used in this study as it is concerned with broad stability relationships between different types of phyllosilicate structure (1:1 and 2:1) and such models are reportedly problematic for some cations (Aagaard and Helgeson, 1983). Thermodynamic models are presented for the system and subsystems of Al_2O_3–FeO–Fe_2O_3–MgO–Na_2O–SiO_2–H_2O where 2:1 and 1:1 phyllosilicates are considered as discrete phases (Table 1). Interstratified layer silicates (reviewed by Środoń, 1999) are not considered here because none of the models available for estimating the thermodynamic properties of clay minerals deal specifically with mixed-layer phases.

The simplified smectite compositions used in this paper have a layer charge of −0.35 as suggested by Deer et al. (1992). The comparison of these simplified mineral formulae to reported mineral formulae (Newman and Brown, 1987; Manceau et al., 2000a; Gates et al., 2002) indicates that this approach is reasonably justified. Minerals with tetrahedral Fe(III) are not included here, since the models available to estimate thermodynamic properties (Holland, 1989; Vieillard, 2000) do not have the capability to include them. Although Fe(II)-rich saponite has not been characterised in much detail, some approximate and hypothetical mineral compositions have been reported which have various tetrahedral Al contents (Kohyama et al., 1973; Kodama et al., 1988). The smectite compositions considered here include Na^+ and Fe^{2+} interlayer cations, since some HLW–EBS designs include Na-exchanged smectite (JNC, 1999) and Fe^{2+} may replace interlayer Na^+ under repository conditions (Kamei et al., 1999). However, other designs may include smectite with interlayer Ca^{2+} or Mg^{2+} and the identity of the interlayer cations present may be altered depending on the chemical composition of the groundwater intruding into the backfill of a given repository.

"The Geochemist's Workbench" software package (Bethke, 1996) was used to carry out the equilibrium calculations required to construct activity diagrams. Ideally, this software can be used to construct activity diagrams that include the most stable configuration of phases. However, the metastability of one phase assemblage relative to another cannot be accurately determined if there are significant uncertainties associated with the data used in the calculations. In preliminary calculations using Geochemists Workbench, all mineral compositions present in the database were included along with the estimated data presented in this paper. Minerals with measured thermodynamic properties that occurred on preliminary phase diagrams included diaspore and albite. Neither of these phases was deemed likely to be produced by clay mineral alteration and they were therefore excluded. The resulting phase assemblages included the mineral compositions given in Table 1.

The standard states used in this work are those incorporated into the software used to calculate the equilibrium constants required for diagram construction (SUPCRT92, Johnson et al., 1992). In summary, the standard states are that pure minerals and pure water have unit activity at all pressures and temperatures; gases have unit fugacity at 1 bar and any temperature; aqueous species have unit activity in a hypothetical 1 molal solution referenced to infinite dilution at any temperature and pressure (Johnson et al., 1992).

2.2. Estimation of Gibbs free energy values (ΔG_f^o) for smectite and 1:1 clay minerals

To calculate the equilibrium constants required for the construction of activity diagrams, estimates of ΔG_f^o were made for Fe-bearing trioctahedral 1:1 phyllosilicates and smectites because experimental values are not available. Several models have been devised for the estimation of ΔG_f^o of clay minerals, based on ideal mixing of end-member clays (Tardy and Fritz, 1981; Tardy and Duplay, 1992), regression techniques (Chen, 1975), polymerisation/polyhedral summation (Tardy and Garrels, 1974; Nriagu, 1975; Mattigod and Sposito, 1978; Chermak and Rimstidt, 1989) and cation electronegativity (Vieillard, 2000, 2002). These methods can be evaluated using two criteria: (1) the degree to which predicted values match measured data and (2) the degree to which the concepts employed by the methods are judged as the most conceptually coherent. In this paper, the coherency of the models is judged on the basis of them adequately treating the different crystallographic sites present in clay minerals (i.e., whether interlayer cations are specifically treated and whether the coordination environment of cations are considered).

The paucity and often questionable quality of the measured thermodynamic data available for clay minerals (May et al., 1986), results in difficulties in using the first criterion. Of the methods available, those presented by Chermak and Rimstidt (1989) and Vieillard (2000, 2002) are deemed the most valid conceptually by the authors of this work. Mixing models were avoided because they use the assumption that mixing is ideal and because the values of end-member solubility products were adjusted to fit experimental data (Tardy and Fritz, 1981).

Chermak and Rimstidt (1989) model seems to be the most elaborate of the polyhedral models because it uses both hydroxide and oxide polyhedrons and takes the effect of cation coordination into account. Chermak and Rimstidt (1989) developed this model by conducting regression analysis on ΔG_f^o values for silicate minerals in order to determine the average contribution of oxide and hydroxide

Table 1
Measured and estimated values of standard molal Gibbs free energy (ΔG_f) heat capacity coefficients (a,b,c) volume (V^o) and "third law" entropy (S^o) of main minerals used in model construction (25 °C, 1 bar)

Idealised mineral	Idealised mineral formulae (half unit cell)	Analogue mineral	(ΔG_f) (J mol^{-1})	a (J mol^{-1} K^{-1})	b ($\times 10^3$) (J mol^{-1} K^{-1})	c ($\times 10^{-5}$) (J mol^{-1} K^{-1})	S^o (J mol^{-1} K^{-1})	V^o (cm^3 mol^{-1})	Estimated properties[a]	Source data[b]
2:1 Smectites										
Na-beidellite	$(Na_{0.35})(Al_2)(Si_{3.65}Al_{0.35})O_{10}(OH)_2$	Marblehead illite	−5358448.5	328.130	215.342	−76.901	255.33	138.42	ΔG_f a b c S^o V^o	—
Na-montmorillonite	$(Na_{0.35})(Al_{1.65}Mg_{0.35})(Si_4)O_{10}(OH)_2$	Marblehead illite	−5305666.9	319.212	225.769	−70.750	260.87	141.35	ΔG_f a b c S^o V^o	—
Na-nontronite	$(Na_{0.35})(Fe_2^{3+})(Si_{3.65}Al_{0.35})O_{10}(OH)_2$	Marblehead illite	−4514326.9	311.394	281.366	−56.692	317.47	143.12	ΔG_f a b c S^o V^o	—
Na–Fe-saponite	$(Na_{0.35})(Fe_3)(Si_{3.65}Al_{0.35})O_{10}(OH)_2$	Marblehead illite	−4589542.2	365.267	229.551	−51.253	367.43	148.84	ΔG_f a b c S^o V^o	—
Na-saponite	$(Na_{0.35})(Mg_3)(Si_{3.65}Al_{0.35})O_{10}(OH)_2$	Marblehead illite	−5592662.2	340.891	225.384	−60.416	279.88	146.59	ΔG_f a b c S^o V^o	—
Fe^{2+}-beidellite	$(Fe_{0.175})(Al_2)(Si_{3.65}Al_{0.35})O_{10}(OH)_2$	Marblehead illite	−5293492.6	323.643	213.279	−75.334	246.71	131.92	ΔG_f a b c S^o V^o	—
Fe^{2+}-montmorillonite	$(Fe_{0.175})(Al_{1.65}Mg_{0.35})(Si_4)O_{10}(OH)_2$	Marblehead illite	−5239746.2	314.725	223.705	−69.183	252.25	134.85	ΔG_f a b c S^o V^o	—
Fe^{2+}-nontronite	$(Fe_{0.175})(Fe_2^{3+})(Si_{3.65}Al_{0.35})O_{10}(OH)_2$	Marblehead illite	−4449371.0	306.907	279.302	−55.125	308.85	136.62	ΔG_f a b c S^o V^o	—
Fe^{2+}–Fe-saponite	$(Fe_{0.175})(Fe_3)(Si_{3.65}Al_{0.05})O_{10}(OH)_2$	Marblehead illite	−4524586.4	360.780	227.488	−49.686	358.80	142.35	ΔG_f a b c S^o V^o	—
Fe^{2+}–Mg-saponite	$(Fe_{0.175})(Mg_3)(Si_{3.65}Al_{0.35})O_{10}(OH)_2$	Marblehead illite	−5527706.2	336.404	223.320	−58.849	271.26	140.09	ΔG_f a b c S^o V^o	—
2:1 Talc–pyrophyllite group										
Pyrophyllite	$Al_2Si_4O_{10}(OH)_2$	—	−5255091.4	332.343	164.071	−72.308	239.32	126.60	None	1
Talc	$Mg_3Si_4O_{10}(OH)_2$	Pyrophyllite	−5523666.6	345.105	174.113	−55.823	260.83	136.25	$\Delta G_f S^o V^o$	1
Minnesotaite	$Fe_3Si_4O_{10}(OH)_2$	Talc	−4490312.7	369.472	178.264	−46.652	361.77	147.86	None	—
2:1 Mica group										
Paragonite	$NaAl_2AlSi_3O_{10}(OH)_2$	Muscovite	−5548034.2	407.647	102.508	110.625	265.79	132.53	a b c S^o	1
2:1 Chlorite group										
Chamosite	$Fe_5Al(AlSi_3)O_{10}(OH)_8$	Clinochlore	−6491560.1	737.263	183.092	−141.503	542.17	213.42	a b c S^o	2
Clinochlore	$Mg_5Al(AlSi_3)O_{10}(OH)_8$	—	−8207765.4	696.636	176.146	−156.774	397.60	207.11	S^o	1
1:1 Trioctahedral group										
Amesite	$(Mg_2Al)(SiAl)O_5(OH)_4$	Chrysotile	−4277902.3	342.711	102.424	−91.128	209.00	102.89	ΔG_f a b c S^o	3
Berthierine	$(Fe_2Al)(SiAl)O_5(OH)_4$	Chrysotile	−3623161.2	358.962	105.202	−85.019	270.05	107.07	ΔG_f a b c S^o	4
Greenalite	$Fe_3Si_2O_5(OH)_4$	Chrysotile	−3058135.0	341.607	136.382	−64.392	316.71	117.85	ΔG_f a b c S^o	5
Lizardite	$Mg_3Si_2O_5(OH)_4$	Chrysotile	−4040246.1	317.231	132.214	−73.555	220.88	107.31	ΔG_f a b c S^o	6
1:1 Dioctahedral group										
Kaolinite	$Al_2Si_2O_5(OH)_4$	Chrysotile	−3789089.0	304.470	122.173	−90.040	203.05	99.52	S^o V^o	1
Framework silicates										
Analcime	$NaAlSi_2O_6{\cdot}H_2O$	—	−3088202.0	223.802	101.002	37.154	234.30	97.10		1

[a] Estimates were made using the methods outlind in the text. Some of these values replace the estimated data provided by Helgeson et al. (1978).
[b] Data sources: (1) Helgeson et al. (1978); (2) Saccocia and Seyfried (1993); (3) Zheng and Bailey (1997); (4) Brindley, 1951; (5) Bailey, 1980; (6) Mellini and Zanazzi, 1987.

polyhedral units to the total ΔG_f^o. This model was used to generate ΔG_f^o values for 1:1 phyllosilicates in this work. Unfortunately, electronegativity models were not available to estimate ΔG_f^o values for 1:1 minerals at the time this work was undertaken. However, they were available to estimate values of ΔG_f^o for smectite minerals.

The estimates of smectite ΔG_f^o used in the study were made with the model of Vieillard (2000). This model was chosen because polyhedral models cannot explicitly account for the contribution of interlayer cations to overall ΔG_f^o. Instead, they either include Gibbs free energy of reaction ΔG_f^o values for ill-defined ion-exchange reactions (Tardy and Garrels, 1974; Mattigod and Sposito, 1978), or they assume that interlayer cations have the same coordination environments typical of non-swelling phyllosilicates (Chermak and Rimstidt, 1989). Unfortunately, such assumptions cannot be thoroughly tested.

Vieillard's model is based on the following expression:

$$\Delta G_f^o = \Delta G_{ox}^o + \sum n_i \Delta G_f^o(M_i O_{x_i}), \quad (1)$$

where ΔG_{ox}^o is the Gibbs free energy of formation of the mineral of interest from constituent oxides and the second term is the Gibbs free energy of formation of the constituent oxides. Each constituent oxide has a cation (M) present in amount i with associated oxygens in amount x_i and n is the number of moles of M oxide present in the smectite formula. The term ΔG_{ox}^o is calculated using the expression (Vieillard, 2000):

$$\Delta G_{ox}^o = -12\left\{\sum_{i=1}^{i=n_s-1}\sum_{j=i+1}^{j=n_s} X_i X_j\left[\Delta_G O = M_i^{z_i}\text{clay} - \Delta_G O = M_j^{z_j}\text{clay}\right]\right\}, \quad (2)$$

where for a given pair of cations in the clay mineral (M_i and M_j), X_i and X_j are the mole fractions of oxygen associated with those cations, $\Delta_G O = M_j^{z_j}$clay is a parameter that characterises the electronegativity of cations M_i and M_j (with charge z) and n_s refers to the number of different cations and sites. The value of ΔG_{ox}^o for each mineral of interest is determined by the summation of several interaction terms $[\Delta_G O = M_i^{z_i}\text{clay} - \Delta_G O = M_j^{z_j}\text{clay}]$ between pairs of constituent cations (i and j). Vieillard (2000) determined the values of $\Delta_G O = M^z$ clay by minimising the difference between ΔG_{ox}^o values calculated using Eq. (2) and those derived from reported equilibrium constants for clay mineral solubility. The constant 12 arises due to smectite minerals having 12 oxygen atoms per half unit cell formula. This model and that developed for mica and chlorites (Vieillard, 2002) seem to give more accurate estimates than other models previously reported in the literature (Vieillard, 2000, 2002).

Several approaches have been suggested to estimate the ΔG_f^o of smectite interlayer water: the concept of "polyhedral" water, which is not smectite specific (Chermak and Rimstidt, 1989); the use of ice polymorphs as proxies for interlayer water (Tardy et al., 1999; Mercury et al., 2001); the use of ΔG_r^o values derived from clay mineral dehydration isotherms (Tardy and Duplay, 1992) and the use of regular mixing model (Ransom and Helgeson, 1994a). Ransom and Helgeson's model is the most thorough and is smectite-specific. It considers that smectite hydration can be represented by a regular solid solution model defined by the expression:

$$\text{hs} \leftrightarrow \text{as} + n_c H_2O, \quad (3)$$

where hs is the hydrated end-member smectite, as is the anhydrous end-member smectite and n_c is the stoichiometric number of moles of interlayer H_2O in one mole of the hydrous component. Hence, this approach considers that there is a fully hydrated smectite end-member with unique and constant interlayer water content. Ransom and Helgeson (1994a, 1995) consider that there may be more interlayer water in smectite than their fully hydrated end-member (corresponding to a two water–layer complex) but they state that this extra water does not differ from bulk water in its energy contribution. This is problematic since subsequent work has shown that smectite can have greater hydration states that may be taken to represent states of apparent energy minima (Huang et al., 1994; Wu et al., 1997; Wilson et al., 2004).

The smectite mineral compositions in this work do not include interlayer H_2O molecules. There are two reasons for this. First, Vieillard (2000) model does not include a ΔG_f^o component for interlayer H_2O contributing to the total ΔG_f^o of the mineral as such. Instead, it includes a contribution to ΔG_f^o related to the hydration of interlayer cations. In effect, this means that the ΔG_f^o values are equal to those for a fully hydrated composition, minus the contribution of $H_2O_{(l)}$. Unfortunately, the number of interlayer H_2O molecules associated with the clays used to generate values for the terms in Vieillard's model could not be determined.

Second, the authors are currently of the opinion that none of the models available to predict the contribution of interlayer water to smectite ΔG_f^o values are sufficiently coherent. The exclusion of interlayer H_2O will clearly add a component of error to phase boundaries on calculated activity diagrams. However, the difference in estimated ΔG_f^o values for anhydrous and fully hydrated smectite end-members (according to Ransom and Helgeson, 1994a, 1995) would range from ~1 to 24 kJ mol^{-1} and therefore, at 25 °C, the error associated with ignoring interlayer water is likely to be of a similar magnitude to that associated with the estimates of smectite ΔG_f^o made using Vieillard's model. The approximate effect of error on the positions of phase boundaries resulting from the uncertainties discussed, is given in Section 4.2.

2.3. Standard molal heat capacity, "third law entropy" and volume of silicate minerals

Three-parameter Maier–Kelley heat capacity coefficients (a, b, c parameters, Maier and Kelley, 1932), entropy (S^o)

and volume (V^o) data for minerals used in the models are given in Table 1, in SUPCRT92 format (Johnson et al., 1992). No measured heat capacity data are available for most 1:1 phyllosilicates and smectite minerals and estimates were made using the "analogue mineral algorithm" method (Helgeson et al., 1978; Ransom and Helgeson, 1994b). This method was also used to generate molal volume data for smectites. Estimates of heat capacity coefficients and standard molal volume for non-stoichiometric 2:1 minerals were made using Marblehead illite as the analogue mineral as suggested by Ransom and Helgeson (1994b). For 1:1 minerals, chrysotile ($Mg_3Si_2O_5(OH)_4$) was used as the analogue mineral for heat capacity estimation whereas clinochlore ($Mg_5Al(AlSi_3)O_{10}(OH)_8$) was used for chamosite ($Fe_5Al(AlSi_3)O_{10}(OH)_8$). The relevant analogue mineral and oxide data were taken from Helgeson et al. (1978) and Ransom and Helgeson (1994b). The molal volumes of 1:1 and chlorite minerals were derived from crystallographic data (Table 1).

Estimates of third law standard molal entropy (S^o) were derived using the volume dependant polyhedral method devised by Holland (1989), rather than the analogue mineral algorithm developed by Helgeson et al. (1978). Both models reproduce measured values of S^o to within approximately 2%. However, the analogue mineral algorithm is conceptually weaker as it requires a correction factor for Fe(II)-bearing minerals, which is determined by measuring differences between estimate and measured data and it does not consider cation coordination. The contribution of magnetic effects to entropy in Fe-bearing minerals was also considered in our calculations (Holland, 1989).

2.4. Solute data and consistency

Models for estimating the thermodynamic properties of minerals use various compilations of thermodynamic data, although most mineral data in SUPCRT92 are taken from Helgeson et al. (1978). Thermodynamic calculations were carried out using both SUPCRT92 (Johnson et al., 1992; 1996 revision of the SUPCRT92 database distributed by J.W. Johnson at Lawrence Livermore National Laboratory) and "The Geochemist's Workbench" (Bethke, 1996). The former includes solute data from Helgeson (1985); Shock and Helgeson (1988); Shock et al. (1989); Pokrovskii and Helgeson (1995) and mineral data from Helgeson et al. (1978). The only significant inconsistency found by the authors is that Vieillard's (2000) model includes different values of ΔG_f^o of Fe^{2+} and Fe^{3+} than those in the SUPCRT92 database. However, the differences are within 1 kJ mol^{-1}, which is within the degree of error typically associated with estimated values of ΔG_f^o for smectite minerals (Vieillard, 2000).

2.5. Summary of uncertainties

The uncertainties associated with the models presented in this paper are: (1) the validity of thermodynamic models including non-stoichiometric phyllosilicates has been questioned; (2) the use of end-member clay compositions may be an oversimplification of real systems (especially mixed layers); (3) for many of the Fe-rich clay minerals of interest, only estimated data are available and the effect that the error associated with such data has on phase boundary positions can only be crudely estimated (see Section 4.2).

3. Methods of phase diagram calculation

Both measured and estimated thermodynamic data were introduced into SUPCRT92 (Johnson et al., 1992), which was used to generate mineral dissolution equilibrium constants (K) at set pressure and temperature values. These were incorporated into the 1996 version of the EQ3/6 database (Wolery, 1979, 1996) which was used with "The Geochemist's Workbench" software (Bethke, 1996) to conduct equilibrium calculations required for logarithmic activity diagram construction.

The EQ3/6 database entry has equilibrium constants for mineral dissolution at set values of temperature and pressure (Table 2). Corresponding pressure values are 1.013 bars at $T < 100$ °C, or those corresponding to the liquid–vapour curve for pure water at $T > 100$ °C. If an equilibrium constant (K) for a reaction was required at a temperature value for which there was no database entry, it was calculated using a temperature dependant polynomial function fitted to $\log K$ values for the reaction between 0 and 300 °C. The database includes reactions whereby minerals dissolve congruently into constituent ions that have the same valency as in the mineral and include H^+, H_2O, and $O_{2(aq)}$. Silicate minerals dissolution reactions are written to include $SiO_{2(aq)}$. The Geochemist's Workbench rearranges such equilibrium expressions to generate those required for phase diagram construction.

The stability limits of water are calculated from the equilibrium constants for water dissociation (Table 3), with $f_{H_{2(g)}}$ being equal to total pressure. The P values used in the calculations are not critical for our models of montmorillonite–Fe reactions, since the calculations assume that the molal volumes of minerals are independent of pressure and temperature (Helgeson et al., 1978). Only values of $f_{O_{2(g)}}$ and $f_{H_{2(g)}}$ are affected by pressure. Pressure in HLW repositories could be higher than the values used in our calculations, but these differences, considering the shallow crustal depth would have little effect on $f_{O_{2(g)}}$ and $f_{H_{2(g)}}$.

The logarithmic activity diagrams presented in this study were constructed at 25 °C (1.013 bars) and 80 °C (1.013 bars) to represent conditions some time after repository closure and initial heat decay, and at 250 °C (40 bars) for the interpretation of hydrothermal experiments (Wilson et al., 2006). The activity diagrams were constructed for smectite with either Na^+ or Fe^{2+} in the interlayer. The diagrams are shown both with and without smectite as a thermodynamic phase, because the thermodynamic status of smectite is in dispute (Aja and Rosenberg, 1992; Essene and Peacor, 1995). The background principles used in

Table 2
Calculated equilibrium constants (log K values) for mineral dissolution reactions

T (°C) P (bars)	Dissolution reaction	0	25	60	100	150	200	250	300
		1.01	1.01	1.01	1.01	4.76	15.54	39.74	85.84
2:1 Smectite group									
Na-beidellite	$Na_{0.35}Al_{2.35}Si_{3.65}O_{10}(OH)_2 + 7.4H^+ = 0.35Na^+ + 2.35Al^{3+} + 3.65SiO_{2(aq)} + 4.7H_2O$	8.472	6.274	2.964	−0.407	−3.927	−6.882	−9.509	−12.015
Na-montmorillonite	$Na_{0.35}Mg_{0.35}Al_{1.65}Si_4O_{10}(OH)_2 + 6H^+ = 0.35Na^+ + 0.35\ Mg^{2+} + 1.65Al^{3+} + 4SiO_{2(aq)} + 4H_2O$	6.919	5.575	3.203	0.687	−1.959	−4.166	−6.117	−7.986
Na-nontronite	$Na_{0.35}Fe_2Al_{0.35}Si_{3.65}O_{10}(OH)_2 + 7.4H^+ + 0.35Na^+ + 2Fe^{3+} + 0.35Al^{3+} + 3.65SiO_{2(aq)} + 4.7H_2O$	−10.301	−10.656	−11.873	−13.345	−15.001	−16.485	−17.917	−19.438
Na–Fe-saponite	$Na_{0.35}Fe_3Al_{0.35}Si_{3.65}O_{10}(OH)_2 + 7.4H^+ = 0.35Na^+ + 3Fe^{2+} + 0.35Al^{3+} + 3.65SiO_{2(aq)} + 4.7H_2O$	20.354	18.219	15.038	11.850	8.600	5.957	3.675	1.521
Na-saponite	$Na_{0.35}Mg_3Al_{0.35}Si_{3.65}O_{10}(OH)_2 + 7.4H^+ = 0.35Na^+ + 3Mg^{2+} + 0.35Al^{3+} + 3.65SiO_{2(aq)} + 4.7H_2O$	36.534	32.992	28.232	23.653	19.097	15.476	12.443	9.700
Fe^{2+}-beidellite	$Fe_{0.175}Al_{2.35}Si_{3.65}O_{10}(OH)_2 + 7.4H^+ = 0.175Fe^{2+} + 2.35Al^{3+} + 3.65SiO_{2(aq)} + 4.7H_2O$	6.569	4.401	1.116	−2.242	−5.765	−8.736	−11.392	−13.935
Fe^{2+}-montmorillonite	$Fe_{0.175}Mg_{0.35}Al_{1.65}Si_4O_{10}(OH)_2 + 6H^+ = 0.175Fe^{2+} + 0.35Mg^{2+} + 1.65Al^{3+} + 4SiO_{2(aq)} + 4H_2O$	5.201	3.871	1.507	−1.014	−3.678	−5.915	−7.904	−9.819
Fe^{2+}-nontronite	$Fe(II)_{0.175}Fe(III)_2Al_{0.35}Si_{3.65}O_{10}(OH)_2 + 7.4H^+ + 0.175Fe^{2+} + 2Fe^{3+} + 0.35Al^{3+}3.65SiO_{2(aq)} + 4.7H_2O$	−12.203	−12.529	−13.720	−15.180	−16.839	−18.339	−19.800	−21.358
Fe^{2+}–Fe-saponite	$Fe_{3.175}Al_{0.35}Si_{3.65}O_{10}(OH)_2 + 7.4H^+ = 3.175Fe^{2+} + 0.35Al^{3+} + 3.65SiO_{2(aq)} + 4.7H_2O$	18.452	16.347	13.190	10.014	6.762	4.103	1.793	−0.399
Fe^{2+}–Mg-saponite	$Fe_{0.175}Mg_3Al_{0.35}Si_{3.65}O_{10}(OH)_2 + 7.4H^+ = 0.175Fe^{2+} + 3Mg^{2+} + 0.35Al^{3+} + 3.65SiO_{2(aq)} + 4.7H_2O$	34.631	31.119	26.384	21.818	17.259	13.621	10.560	7.780
2:1 Talc–pyrophyllite group									
Pyrophyllite	$Al_2Si_4O_{10}(OH) + 6H^+ = 2Al^{3+} + 4SiO_{2(aq)} + 4H_2O$	1.634	0.440	−1.785	−4.197	−6.778	−8.970	−10.942	−12.856
Talc	$Mg_3Si_4O_{10}(OH)_2 + 6H^+ = 3Mg^{2+} + 4SiO_{2(aq)} + 4H_2O$	23.110	21.138	18.112	15.085	12.052	9.653	7.647	5.805
Minnesotaite	$Fe_3Si_4O_{10}(OH)_2 + 6H^+ = 3Fe^{2+} + 4SiO_{2(aq)} + 4H_2O$	12.776	11.662	9.585	7.373	5.081	3.215	1.601	0.053
2:1 Chlorite group									
Chamosite	$Fe_5Al_2Si_3O_{10}(OH)_8 + 16H^+ = 5Fe^{2+} + 2Al^{3+} + 3SiO_{2(aq)} + 12H_2O$	57.917	50.386	41.113	32.410	23.685	16.565	10.398	4.679
Clinochlore	$Mg_5Al_2Si_3O_{10}(OH)_8 + 16H^+ = 5Mg^{2+} + 2Al^{3+} + 3SiO_{2(aq)} + 12H_2O$	76.411	67.239	56.144	45.862	35.686	27.509	20.552	14.234
2:1 Mica group									
Paragonite	$NaAl_3Si_3O_{10}(OH)_2 + 10H^+ = Na^+ + 3Al^{3+} + 3SiO_{2(aq)} + 6H_2O$	21.589	17.522	12.195	7.044	1.784	−2.573	−6.399	−9.983
1:1 Trioctahedral group									
Amesite	$Mg_2Al_2SiO_5(OH) + 10H^+ = 2Mg^{2+} + 2Al^{3+} + SiO_{2(aq)} + 7H_2O$	21.656	17.341	12.173	7.390	2.614	−1.306	−4.746	−7.984
Berthierine	$Fe_2Al_2SiO_5(OH)_4 + 10H^+ = 2Fe^{2+} + 2Al^{3+} + SiO_{2(aq)} + 7H_2O$	8.204	5.038	1.167	−2.467	−6.154	−9.250	−12.049	−14.778
Greenalite	$Fe_3Si_2O_5(OH)_4 + 6H^+ = 3Fe^{2+} + 2SiO_{2(aq)} + 5H_2O$	13.651	12.107	9.962	7.882	5.800	4.118	2.654	1.242
Lizardite	$Mg_3Si_2O_5(OH)_4 + 6H^+ = 3Mg^{2+} + 2SiO_{2(aq)} + 5H_2O$	33.808	30.560	26.495	22.713	19.018	16.115	13.702	11.537
1:1 Dioctahedral group									
Kaolinite	$Al_2Si_2O_5(OH)_4 + 6H^+ = 2Al^{3+} + 2SiO_{2(aq)} + 5H_2O$	9.018	6.810	3.847	0.954	−2.019	−4.502	−6.708	−8.802
Framework silicates									
Analcime	$NaAlSi_2O_6{:}H_2O{+}4H^+ = Na^+ + Al^{3+} + 2SiO_{2(aq)} + 3H_2O$	8.104	6.948	5.222	3.494	1.736	0.309	−0.920	−2.068
(Hydro)oxides									
Amorphous Silica	$SiO_{2(am)} = SiO_{2(aq)}$	−3.124	−2.714	−2.407	−2.184	−1.980	−1.819	−1.693	−1.604
Quartz	$SiO_{2(qz)} = SiO_{2(aq)}$	−4.632	−3.999	−3.473	−3.078	−2.719	−2.438	−2.206	−2.017
Magnetite	$Fe_3O_4 + 8H^+ = Fe^{2+} + 2Fe^{3+} + 4H_2O$	13.899	10.472	6.442	2.691	−1.125	−4.332	−7.207	−9.952
Hematite	$Fe_2O_3 + 6H^+ = 2Fe^{3+} + 3H_2O$	2.141	0.109	−2.318	−4.607	−6.978	−9.021	−10.904	−12.751
Green Rust (Cl)	$Fe(II)_3Fe(III)(OH)_8Cl{+}8H^+ = 3Fe^{2+} + Fe^{3+} + Cl^- + 8H_2O$		24.707						
Native elements									
Fe	$Fe{+}2H^+ + 0.5O_{2(aq)} = Fe^{2+} + H_2O$	64.970	59.033	52.159	45.837	39.557	34.534	30.379	26.823

Table 3
Log $f_{O_{2(g)}}$ values dictated by equilibrium reactions in the system Fe–O–H

Fe-magnetite equilibrium: $1.5Fe + O_{2(g)} = 0.5Fe_3O_4$						
T (°C)	25.00	80.00	250.00	25.00	80.00	250.00
P (bars)	1.01	1.01	39.74	500.00	500.00	500.00
Log $f_{O_{2(g)}}$	−88.90	−73.63	−46.86	−88.85	−72.61	−46.84
Magnetite–hematite equilibrium: $4Fe_3O_4 + O_{2(g)} = 6Fe_2O_3$						
T (°C)	25.00	80.00	250.00	25.00	80.00	250.00
P(bars)	1.01	1.01	39.74	500.00	500.00	500.00
Log $f_{O_{2(g)}}$	−72.30	−58.90	−35.30	−72.27	−58.88	−35.28
Water dissociation: $2H_2O = 2H_{2(g)} + O_{2(g)}$						
T (°C)	25.00	80.00	250.00	25.00	80.00	250.00
P (bars)	1.01	1.01	39.74	500.00	500.00	500.00
Log K	−83.11	−67.52	−40.46	−82.79	−67.28	−40.25
Log $f_{O_{2(g)}}$	−83.12	−67.53	−43.65	−88.19	−72.68	−45.65

defining equilibrium boundaries in activity space are discussed in detail elsewhere (e.g., Garrels and Christ, 1965; Bowers et al., 1984).

4. Modelling results

4.1. Fe-(hydr)oxide stability

Several Fe-(hydr)oxide minerals may be produced by steel corrosion. In general, the most commonly reported include magnetite, lepidocrocite and goethite (Antunes et al., 2003) although "green rust" minerals (double layered hydroxyl salt compounds, Génin et al., 2001) may occur with magnetite (e.g., Refait et al., 2003a) and may be magnetite precursors (Tamaura et al., 1984).

The scenario modelled in this paper, is of a HLW repository situated at depth below the water table, where the Fe present in steel does not oxidise directly to Fe(III) to produce minerals like goethite. If corrosion of steel to Fe(III) oxyhydroxides occurred, it seems unlikely that significant amounts of iron could be released to solution to react with the montmorillonite present (unless pH was very low). Depending upon pore water pH, the oxidation of Fe could produce Fe^{2+} and mixed valence iron-(hydr)oxides possibly with the production of $H_{2(g)}$and low $f_{O_{2(g)}}$ conditions (Table 3).This would probably only occur if dissolved oxygen present in bentonite pore water was rapidly consumed. Under acidic to mildly alkaline pH conditions, the following reaction could occur:

$$Fe_{(s)} + 2H^+ \leftrightarrow Fe^{2+} + H_{2(g)} \quad (4)$$

and at higher pH values, Fe may oxidise to magnetite

$$3Fe_{(s)} + 4H_2O_{(l)} \leftrightarrow Fe_3O_{4(s)} + 4H_{2(g)}. \quad (5)$$

Green rust minerals and/or magnetite, could be further oxidised to maghemite or Fe(III)-(hydr)oxides such as ferrihydrite depending on $H_{2(g)}$ diffusion and the chemistry of the intruding host rock pore water. These minerals are likely to have small and relatively disordered crystals, and minerals such as ferrihydrite are likely to recrystallise to higher-stability goethite and/or hematite (Schwertmann and Murad, 1983; Schwertmann and Fechter, 1994; Refait et al., 2003b).

The activities of Fe^{2+} that will develop in a HLW repository will affect mineral stabilities. With the low fluid flux expected in bentonite barrier, Fe^{2+} activities are likely to approach saturation with respect to canister corrosion products such as green rust or magnetite. In order to compare the solubilities of a green rust mineral and magnetite, the activities of Fe^{2+} corresponding to green rust and magnetite saturation were computed as a function of pH at $f_{O_{2(g)}}$ conditions corresponding to magnetite–hematite equilibrium (Fig. 3). Using Cl-bearing green rust as an example, its solubility is defined by the reaction

$$Fe_3^{(II)}Fe^{(III)}(OH)_8Cl + 7H^+ \leftrightarrow 4Fe^{2+} + 7.5H_2O + Cl^- + 0.25O_{2(g)} \quad (6)$$

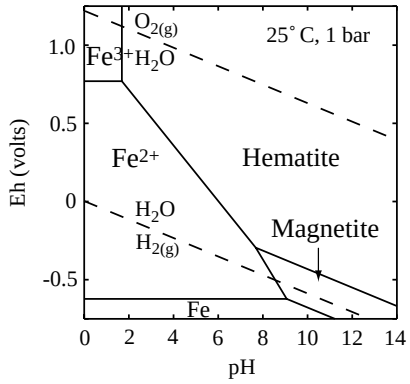

Fig. 2. Eh–pH diagrams for the system FeO–Fe_2O_3–H_2O, calculated at 25 °C, 1.013 bar, $a_{H_2O} = 1$, $a_{Fe^{2+}} = 10^{-5}$.

Table 4
Equilibrium constants used to calculate magnetite solubility

T (°C)	P (bars)	Log K	Log $f_{O_{2(g)}}$	Log$(a_{Fe^{2+}}/(a_{H^+})^2)$
25.00	1.01	−5.06	−82.12	12.00
80.00	1.01	−5.49	−66.53	9.26
150.00	4.75	−5.88	−54.05	7.05
250.00	39.74	−6.56	−42.65	4.92
25.00	1.01	−5.06	−72.30	10.36
80.00	1.01	−5.49	−58.90	7.99
150.00	4.75	−5.88	−46.90	5.85
250.00	39.74	−6.56	−35.30	3.70

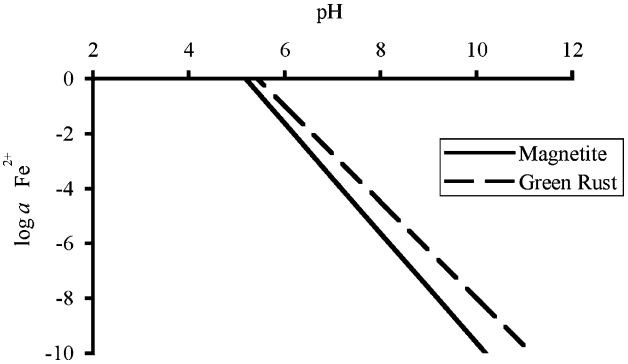

Fig. 3. Magnetite and chlorinated green rust solubility plots, at 25 °C, 1 bar, green rust solubility was calculated with $a_{Cl^-} = 10^{-3}$, $f_{O_{2(g)}} = -72.3$ (magnetite–hematite buffer).

this was rearranged assuming unit water and mineral activities to give the expression for Fe^{2+}

$$\log a_{Fe^{2+}} = \tfrac{1}{4}\log K_{Eq.(6)} - 1.75\mathrm{pH} - \tfrac{1}{4}\log a_{Cl^-} - 1/16\log f_{O_{2(g)}}. \quad (7)$$

The equilibrium solubility of magnetite is defined by

$$Fe_3O_4 + 6H^+ \leftrightarrow 3Fe^{2+} + 3H_2O + \tfrac{1}{2}O_{2(g)} \quad (8)$$

which may be rearranged to give

$$\log a_{Fe^{2+}} = \tfrac{1}{3}\log K_{Eq.(8)} - \tfrac{1}{6}\log f_{O_{2(g)}} - 2\mathrm{pH} \quad (9)$$

Thermodynamic data for green rust was taken from Bourrié et al. (1999), for magnetite from Helgeson et al. (1978) and solute data were taken from SUPCRT96 database. The plot of the activity of $Fe^{2+}_{(aq)}$ at saturation (Fig. 3) suggests that under alkaline pH conditions the presence of green rust would result in higher Fe^{2+} activities than those expected with magnetite. The activity of Cl^- has little relative effect on chlorinated green rust solubility. For example, at pH 8, 25 °C, 1 bar and $\log f_{O_{2(g)}} = -72.3$ (magnetite–hematite equilibrium), the $\log a_{Fe^{2+}}$ value ranges from −5.271 to −5.246 when $\log a_{Cl^-}$ ranges from −1 to −4.

Since green rust is found to act as a magnetite precursor and is stable only under extremely low Eh conditions

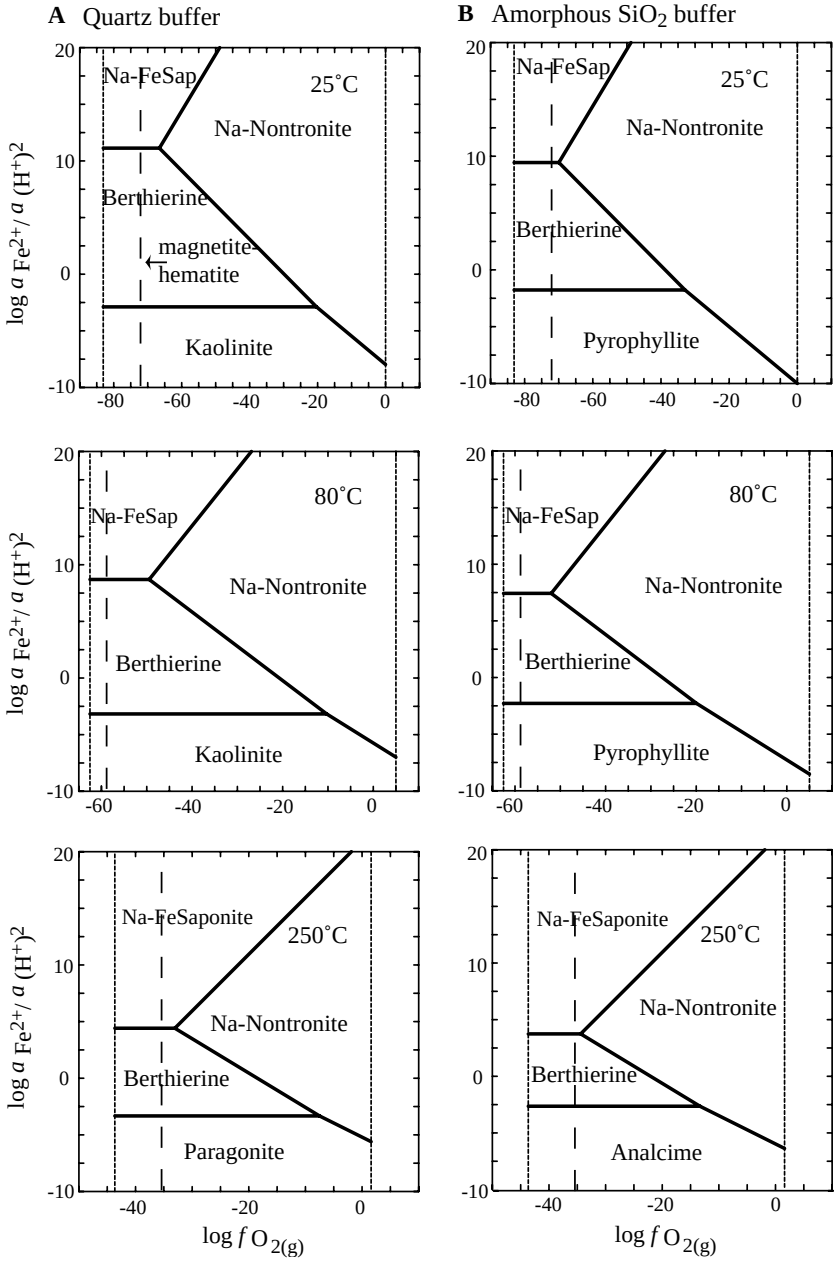

Fig. 4. Logarithmic activity diagrams for the system Al_2O_3–FeO–Fe_2O_3–Na_2O–SiO_2–H_2O including Na-smectite, with $SiO_{2(aq)}$ buffered by quartz (A) and amorphous silica (B). All diagrams were calculated with $a_{H_2O} = 1$ and $\log(a_{Na^+}/a_{H^+}) = 5$. The dashed line represents $f_{O_{2(g)}}$ corresponding to magnetite–hematite equilibrium. See Table 2 for mineral compositions.

(below the stability limit of water, Fig. 2), values of $\log(a_{Fe^{2+}}/(a_{H^+})^2)$ corresponding to magnetite rather than green rust saturation are included on the logarithmic activity diagrams presented here. These values were calculated at different values of T, P and $f_{O_{2(g)}}$ (Table 4 and Fig. 3).

4.2. Results of mineral–fluid equilibrium calculations

Models of mineral–fluid equilibria in the system and subsystems of Al_2O_3–FeO–Fe_2O_3–MgO–Na_2O–SiO_2–H_2O are given in Figs. 4–8. Most of the diagrams constructed assume that dissolved silica activity is buffered by quartz solubility, according to the reaction:

$$SiO_{2(quartz)} \leftrightarrow SiO_{2(aq)} \quad (10)$$

The diagrams given in Fig. 4 include only Na-exchanged smectite ($(\log a_{Na^+}/a_{H^+}) = 5$) and it includes diagrams where silica activity is buffered by quartz and amorphous silica (Fig. 4). Activity diagrams constructed with amorphous silica buffered reactions have boundaries between berthierine and Na-exchanged Fe(II)-saponite at lower $\log(a_{Fe^{2+}}/(a_{H^+})^2)$ values than quartz-buffered reactions.

Plots of $\log(a_{Fe^{2+}}/(a_{H^+})^2)$ versus $\log(a_{Na^+}/a_{H^+})$ were generated including Na^+-saturated smectite (Fig. 5A), Fe^{2+}-exchanged smectite (Fig. 5B), no smectite (Fig. 6A) and no smectite or berthierine (Fig. 6B). They show that in the system Al_2O_3–FeO–Na_2O–SiO_2–H_2O, the most stable phases of those considered are kaolinite, berthierine, Fe(II)-saponite, paragonite and analcime (Fig. 5). Although the stability fields of both Na- and Fe^{2+}-

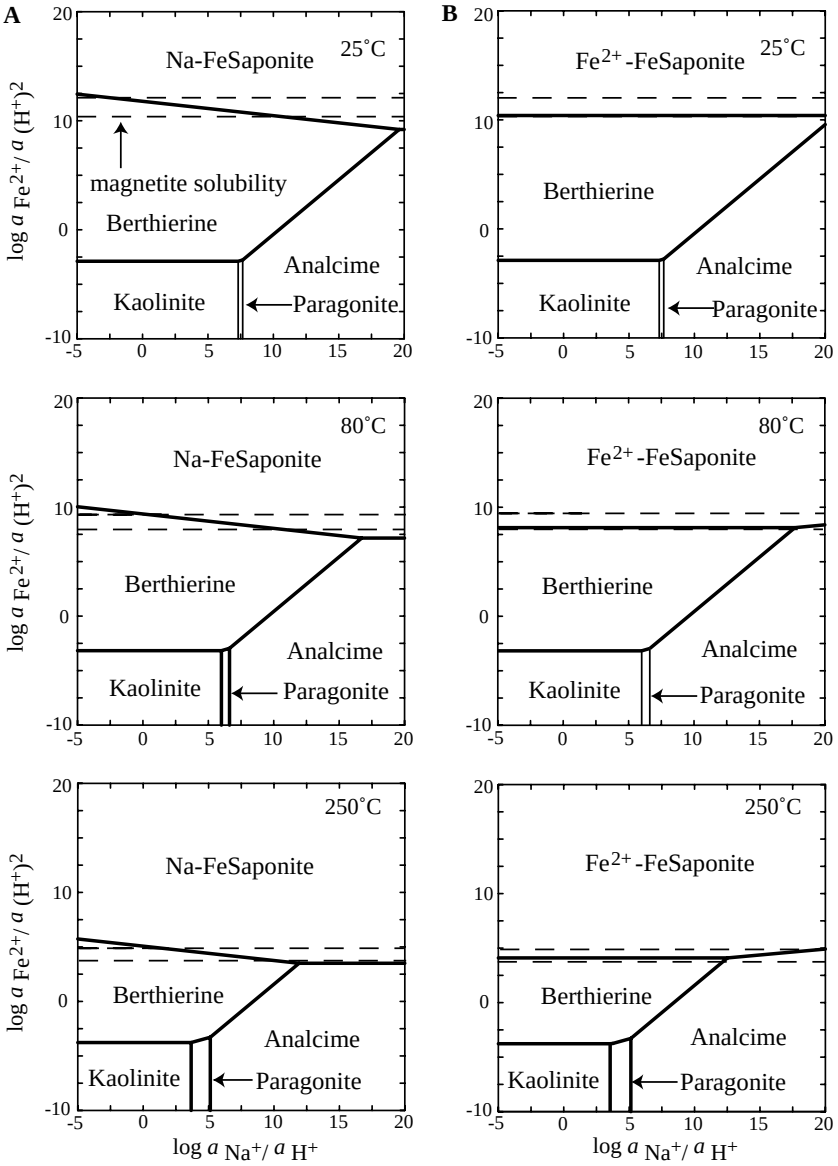

Fig. 5. Logarithmic activity diagrams for the system Al_2O_3–FeO–Na_2O–SiO_2–H_2O including Na-smectite (column A) and Fe^{2+}-smectite (column B). All diagrams were calculated with $a_{H_2O} = 1$. The dashed lines mark the equilibrium solubility of magnetite at $f_{O_{2(g)}}$ corresponding to both $H_{2(g)}$–$H_2O_{(l)}$ equilibrium (upper) and magnetite–hematite equilibrium (lower).

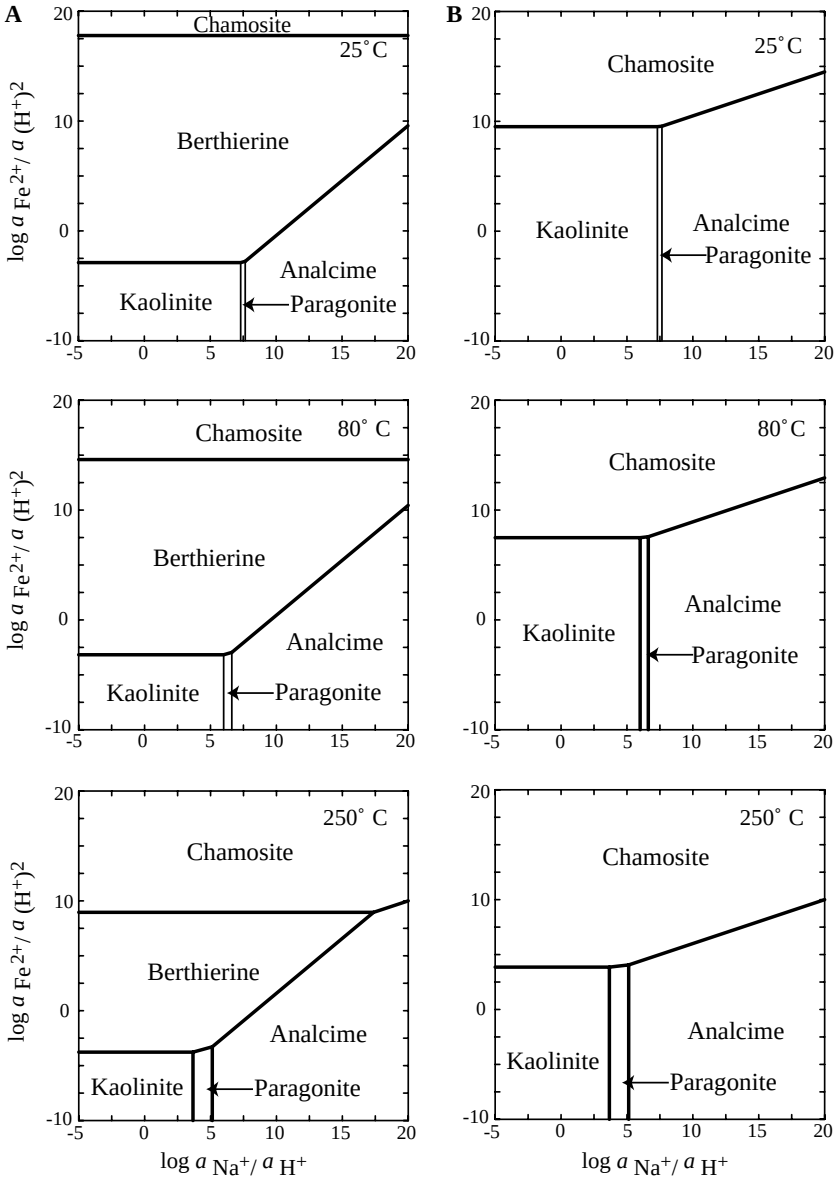

Fig. 6. Logarithmic activity diagrams for the system Al_2O_3–FeO–H_2O–Na_2O–SiO_2, excluding smectite (column A) and excluding smectite and berthierine (column B).

exchanged smectite are similar, the slope of the boundary between Fe(II)-saponite and berthierine is different, due to the different smectite stoichiometries (Fig. 5). If smectite is excluded from the models, chamosite and berthierine replace it (Fig. 6A). If berthierine is also excluded, it is replaced by kaolinite, with chamosite replacing Fe(II)-saponite (Fig. 6B).

The errors associated with the phase boundaries on the activity diagrams can only be crudely approximated at 25 °C. The systematic and random components of error in the calculations cannot be explicitly stated and even if they were clear, the propagation of error through all calculations is beyond the scope of this work. However, at 25 °C, 1 bar, a crude estimate of the error in the position of the boundary between berthierine and Fe(II)-saponite can be generated. The position of the boundary between these two phases can be estimated by calculating the equilibrium constant for the following equilibrium expression:

$$\underset{\text{(berthierine)}}{(Fe_2Al)(SiAl)O_5(OH)_4} + 19.856\underset{\text{(quartz)}}{SiO_{2(s)}} + 15.142Fe^{2+} + 2Na^+ + 19.856H_2O = \underset{\text{(Na–Fe(II)-Saponite)}}{5.714Na_{0.35}Fe_3Si_{3.65}Al_{0.35}O_{10}(OH)_2} + 32.284H^+ \quad (11)$$

which is given by

$$\log K_{\text{Eq.}(11)} = -15.14 \log a_{[Fe^{2+}/(H^+)^2]} - 2 \log a_{[Na^+/H^+]} \quad (12)$$

The methods used to estimate the ΔG_f^o of the berthierine and Fe(II)-saponite appear to give predictions generally to within ~0.25% of measured values (Chermak and Rimstidt, 1989; Vieillard, 2000). The approximate error associated with ΔG_r^o for Eq. (11) may be estimated by: multiplying

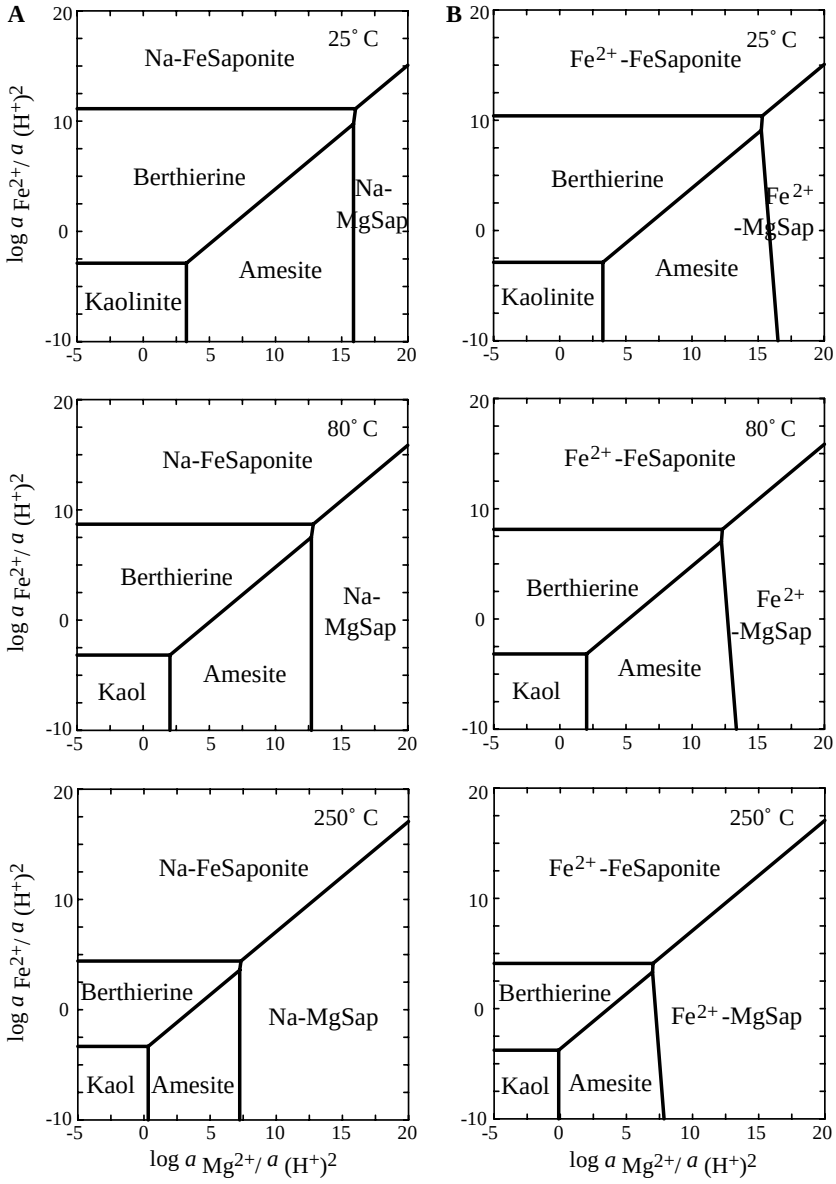

Fig. 7. Logarithmic activity diagrams for the system Al_2O_3–FeO–H_2O–MgO–Na_2O–SiO_2 including Na-smectite (column A, $\log(a_{Na^+}/a_{H^+}) = 5$) and Fe^{2+}-smectite (column B).

the estimated ΔG_f^o of each mineral by 0.0025; multiplying each of these values by the relevant stoichiometric coefficient for the reaction defined in Eq. (11), and finally taking the square root of the sum of the two calculated error contributions. At 25 °C, 1 bar, this gives an approximate error of 66 kJ mol^{-1} for the ΔG_r^o defined in Eq. (11). This error represents an error of 0.8 log units on the *y*-axis $\log a_{Fe^{2+}/(H^+)^2}$. The errors associated with the phase boundaries for the end-member compositions chosen are therefore not insignificant, however, given the range required on the axes to show the stability fields of the minerals of interest, they are not of a large enough magnitude to render the diagrams meaningless for the purposes of this study.

For Mg-bearing systems, plots were calculated with Na^+-exchanged smectite (Fig. 7A), Fe^{2+}-exchanged smectite (Fig. 7B), without smectite (Fig. 8A) and without smectite or berthierine (Fig. 8B). In this case, the positions of phase boundaries are similar, but Mg saponite is stable at high values of $\log(a_{Mg^{2+}}/(a_{H^+})^2)$ and amesite is present (Fig. 7A). Mg-saponite is replaced by clinochlore and amesite when smectite minerals are excluded (Fig. 8A). If berthierine is excluded from the diagrams, (Figs. 6B, 8B) it is replaced by both kaolinite and chamosite. In all plots (Figs. 4–7) berthierine and amesite stability fields decrease in size with increasing temperature.

Calculated values of $\log(a_{Fe^{2+}}/(a_{H^+})^2)$ for magnetite saturation are generally near the boundaries between Fe(II)-rich saponite and berthierine (dashed lines in Fig. 5) when $f_{O_{2(g)}}$ is between H_2–H_2O and Fe_3O_4–Fe_2O_3 equilibrium. Hence, for Fe-rich smectite to be stable, the fluid in contact with it must be saturated with respect to magnetite. Overall, the activity diagrams show that a high activity of

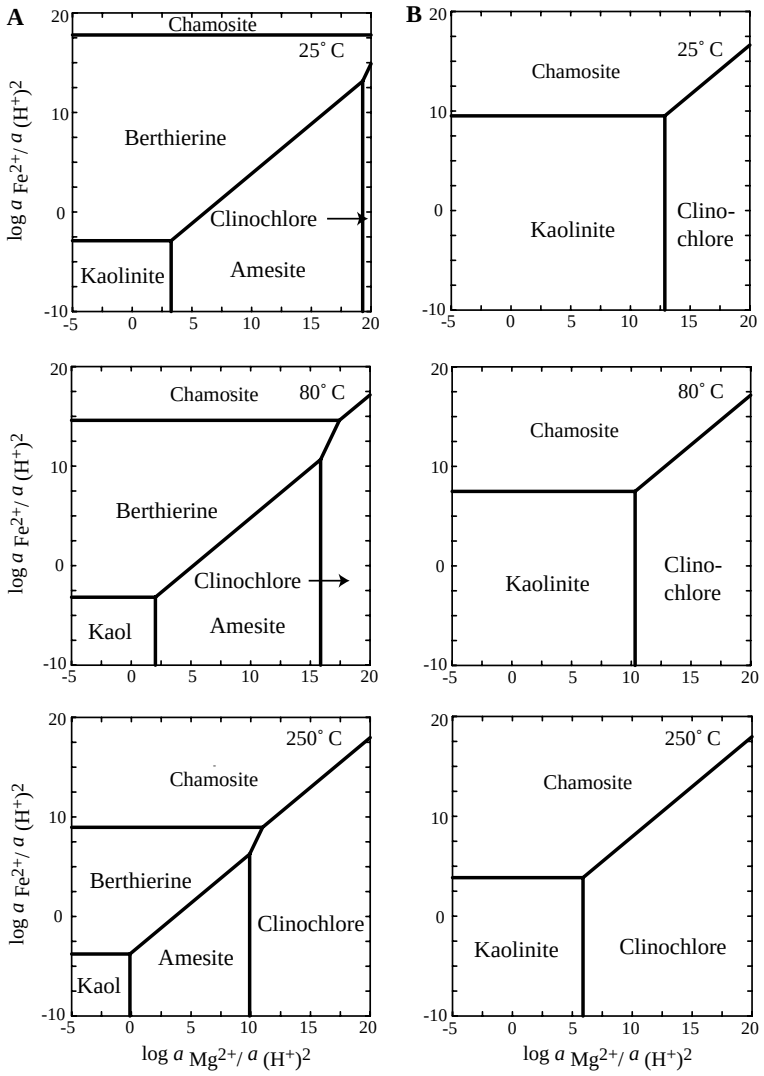

Fig. 8. Logarithmic activity diagrams for the system Al_2O_3–FeO–H_2O–MgO–SiO_2 excluding smectite (column A), and excluding smectite and berthierine (column B).

Na^+ is required in order for Na tectosilicates to be more stable than Fe-rich phyllosilicates. For example, the lowest value of $\log(a_{Na^+}/a_{H^+})$ under which Na-tectosilicates will be more stable than Fe-rich clays (berthierine–paragonite–kaolinite junction) is approximately 7.5 at 25 °C (Figs. 5 and 6). At pH 6–9, this corresponds to a Na^+ activity of between 0.0158 and 15.8, which even with an activity coefficient of 0.5 corresponds to a minimum Na concentration of $\sim$180 mg l^{-1}.

5. Discussion: Implications of thermodynamic models for bentonite stability in HlW repositories

Given the uncertainties associated with the thermodynamic modelling of clay mineral stability and the wide variety in clay mineral composition and structure, it is not possible to determine exactly the stability fields of Fe-rich silicates in water-saturated systems. However, the general trends seen in the models presented in this work give broad indications of the conditions under which different Fe-rich sheet silicate minerals are likely to be (meta)stable. Experimental studies are required to test the thermodynamic models presented in this paper and to measure the kinetics of montmorillonite alteration reactions.

The results of the calculations depend on whether smectite minerals and even 1:1 minerals are classed as true thermodynamic phases. In our opinion, the inclusion of these minerals in thermochemical models is a more realistic approach in trying to account for the results of hydrothermal experiments and to attempt to predict probable reaction pathways in HLW repositories, even if there are conceptual and practical difficulties.

Overall, the models presented in this paper suggest that under the $f_{O_{2(g)}}$ conditions that are likely to occur in a HLW–EBS repository (between water stability and magnetite–hematite equilibrium), montmorillonite is more likely to undergo alteration to Fe(II)-saponite than nontronite. They also suggest that the higher the activity of $SiO_{2(aq)}$,the

more likely it is that Fe(II)-saponite will be favoured over berthierine with the condition that water is saturated or supersaturated with respect to magnetite. The alteration of montmorillonite to Na-tectosilicates only seems likely under high Na^+ activities, such as those expected of brackish or saline environments. Hence, the two most likely candidate montmorillonite alteration products are Fe(II)-saponite and berthierine and their relative stabilities will depend on pH, Fe^{2+}, and $SiO_{2(aq)}$ activities.

Although the models presented here include only Na^+ and Fe^{2+}-exchanged smectite, the identity of the predominant interlayer cation(s) in a HLW repository will depend upon factors such as solute activities in intruding groundwater and pH since smectite exhibits acid–base properties which depend on reactions involving both ion-exchange sites and amphoteric hydroxyl groups (Wanner et al., 1994; Baeyens and Bradbury, 1997). One potential reaction pathway is that Fe^{2+} could replace interlayer Na^+ resulting in relatively lower values of $(\log a_{Fe^{2+}}/(a_{H^+})^2)$ corresponding to the stability field of berthierine, thereby promoting montmorillonite replacement with a non-swelling mineral.

The results of the hydrothermal experiments presented in the companion paper of this study show that the simplified models do broadly predict the nature of alteration of montmorillonite in the presence of Fe. In experiments conducted at 250 °C ($P = P_{sat}$), starting mixtures that included native Fe, montmorillonite and NaCl solutions, produced magnetite and Fe-rich smectite. The solute activities calculated from measured concentrations plot in the stability field of simplified Na-saturated Fe(II)-saponite. An experiment where montmorillonite was reacted with native Fe and $FeCl_2$ solutions at 250 °C, did not produce significant quantities of Fe-rich smectite. Instead, the montmorillonite included in the starting mixture appeared to undergo minor alteration to a 1:1-type clay mineral. In this experiment, solute activities plotted in the berthierine stability field.

In conclusion, simplified thermodynamic models appear to provide an indication of the likely reactions between iron and montmorillonite under given solute activities. However, the problems associated with measured and estimated thermodynamic data for clay minerals and the issues surrounding the conceptual validity of modelling the relative stabilities of clay minerals using thermodynamics (May et al., 1986; Aja and Rosenberg, 1992; Essene and Peacor, 1995) are likely to continue to capture the attention of the geochemical community. It is currently the authors' opinion that at present, the only viable approach to understanding clay mineral stability, given the data currently available, is to continue to refine estimation techniques so as to generate thermodynamic approximations which have a lower degree of uncertainty and to compare these to experimental or well-constrained data from natural systems. However, whether this will ultimately lead to a full understanding the stability of clays is not clear at the present time. It is hoped that the work presented in this paper and its companion will stimulate further research in these areas.

Acknowledgments

The senior author acknowledges funding from NERC (Ph.D. studentship) and Japan Nuclear Cycle Development Institute for CASE studentship support through Quintessa Ltd. The authors would like to thank Philippe Vieillard for his advice and assistance. E. Gaucher, P. Blanc, C. Tournassat, two anonymous reviewers and the associate editor E.H.Oelkers are thanked for their comments which greatly improved the manuscript.

Associate editor: Eric. H. Oelkers

References

Aagaard, P., Helgeson, H.C., 1983. Activity/composition relationships among silicates and aqueous solutions, II Chemical and thermodynamic consequences of ideal mixing of atoms on homological sites in montmorillonites, illites and mixed-layer clays. *Clays Clay Miner.* **31**, 207–217.

Aagaard, P., Jahren, J.S., Harstad, A.O., Nilsen, O., Ramm, M., 2000. Formation of grain-coating chlorite in sandstones. Laboratory synthesized vs. natural occurrences. *Clay Miner.* **35**, 261–269.

Ahn, J.H., Peacor, D.R., 1995. Transmission electron microscopy study of diagenetic chlorite in Gulf Coast argillaceous sediments. *Clays Clay Miner.* **43**, 228–236.

Aja, S.U., Rosenberg, P.E., 1992. The thermodynamic status of compositionally variable clay minerals—a discussion. *Clays Clay Miner.* **40**, 292–299.

Aja, S.U., Rosenberg, P.E., 1996. The thermodynamic status of compositionally complex clay minerals: discussion of "Clay Mineral Thermometry—a critical perspective". *Clays Clay Miner.* **44**, 560–568.

Antunes, R.A., Costa, I., de Faria, D.L.A., 2003. Characterisation of corrosion products formed on steels in the first months of atmospheric exposure. *Mater. Res.* **6**, 403–408.

Apted, M., 1995. Repository and barrier concepts. In: Savage, D. (Ed.), *The Scientific and Regulatory Basis for the Geological Disposal of Radioactive Wastes*. Wiley, Chichester.

Badaut, D., Besson, D., Decarreau, A., Rautureau, R., 1985. Occurrence of a ferrous trioctahedral smectite in recent sediments of Atlantis II Deep, Red Sea. *Clay Miner.* **20**, 389–404.

Bailey, S.W., 1980. Structures of layer silicates. In: Brindley, G.W., Brown, G. (Eds.), *Crystal Structures of Clay Minerals and Their X-ray Identification*. Mineralogical Society, London.

Baeyens, B., Bradbury, M.H., 1997. A mechanistic description of Ni and Zn sorption on Na-montmorillonite. Part 1: titration and sorption measurements. *J. Contam. Hydrol.* **27**, 199–222.

Beaufort, D., Meunier, A., 1994. Saponite, corrensite and chlorite–saponite mixed-layers in the Sancerre-Couy deep drill hole, France. *Clay Miner.* **29**, 47–61.

Bethke, C.M., 1996. *Geochemical Reaction Modeling*. Oxford University Press, Oxford.

Bischoff, J.L., 1972. A ferroan nontronite from the Red Sea geothermal system. *Clays Clay Miner.* **20**, 217–233.

Bourrié, G., Trolard, F., Génin, J.-M.R, Jaffrezix, A., Maître, V., Abdelmoula, M., 1999. Iron control by equilibria between hydroxygreen rusts and solutions in hydromorphic soils. *Geochim. Cosmochim. Acta* **63**, 3417–3427.

Bowers, T.S., Jackson, K.J., Helgeson, H.C., 1984. *Equilibrium Activity Diagrams for Coexisting Minerals and Aqueous Solutions at Pressures and Temperatures to 5 kb and 600 °C*. Springer-Verlag, Berlin.

Brindley, G.W., 1951. The crystal structure of some chamosite minerals. *Miner. Mag.* **29**, 502–525.

Bucher, F., Spiegel, U. 1984. Quelldruck von hochverdichteten bentoniten. NTB 84-18. Nagra, Hardstrasse 73, CH-5430 Wettingen, Schweiz.

Chen, C-H., 1975. A method of estimation of standard free energies of formation of silicate minerals at 298.15 K. *Am. J. Sci.* **275**, 801–817.

Chermak, J.A., Rimstidt, J.D., 1989. Estimating the thermodynamic properties of silicate minerals at 298 K from the sum of polyhedral contributions. *Am. Mineral.* **74**, 1023–1031.

Deer, W.A., Howie, R.A., Zussman, J., 1992. *An Introduction to the Rock Forming Minerals*, second ed. Longman, Harlow.

Drits, V.A., Manceau, A., 2000. A model for the mechanism of Fe^{3+} to Fe^{2+} reduction in dioctahedral smectites. *Clays Clay Miner.* **48**, 185–195.

Essene, E.J., Peacor, D.R., 1995. Clay mineral thermometry—a critical perspective. *Clays Clay Miner.* **43**, 540–553.

Essene, E.J., Peacor, D.R., 1997. Illite and smectite: metastable, stable or unstable. Further discussion and a correction. *Clays Clay Miner.* **45**, 116–122.

Garrels, R.M., Christ, C.L., 1965. *Solutions, Minerals and Equilibria*. Harper, London.

Gates, W.P., Slade, P.G., Manceau, A., Lanson, B., 2002. Site occupancies by iron in nontronites. *Clays Clay Miner.* **50**, 223–239.

Génin, J.-M.R., Refait, P., Bourrié, G., Abdelmoula, M., Trolard, F., 2001. Structure and stability of the Fe(II)–Fe(III) green-rust "fougerite" mineral and its potential for reducing pollutants in soil solutions. *Appl. Geochem.* **16**, 559–570.

Grauer, R., 1994. Bentonite as a backfill material in a high-level waste repository. *Mater. Res. Bull.*, 43–46.

Helgeson, H.C., Delany, J.M., Nesbitt, H.W., Bird, D.K., 1978. Summary and critique of the thermodynamic properties of rock-forming minerals. *Am. J. Sci.* **278A**.

Helgeson, H.C., 1985. Errata II. Thermodynamics of minerals, reactions, and aqueous solutions at high pressures and temperatures. *Am. J. Sci.* **285**, 845–855.

Hillier, S., Velde, B., 1992. Chlorite interstratified with a 7 Å mineral, an example from offshore Norway and possible implications for the interpretation of the composition of diagenetic chlorites. *Clay Miner.* **24**, 475–486.

Holland, T.J.B., 1989. Dependence of entropy on volume for silicate and oxide minerals—a review and a predictive model. *Am. Mineral.* **74**, 5–13.

Huang, W.-L., Bassett, W.A., Wu, T.C., 1994. Dehydration and hydration of montmorillonite at elevated temperatures and pressures monitored using synchotron radiation. *Am. Mineral.* **79**, 683–691.

Inoue, A., Utada, M., 1991. Smectite-to-chlorite transformation in thermally metamorphosed volcanoclastic rocks in the Kamkita area, northern Honshu, Japan. *Am. Mineral.* **76**, 628–640.

Jiang, W.-T., Peacor, D.R., Slack, J.F., 1992. Microstructures, mixed layering, and polymorphism of chlorite and retrograde berthierine in the Kidd Creek Massive Sulphide deposit, Ontario. *Clays Clay Miner.* **40**, 501–514.

Jiang, W.-T., Peacor, D.R., 1994. Prograde transitions of corrensite and chlorite in low-grade pelitic rocks from the Gaspe Peninsula, Quebec. *Clays Clay Miner.* **42**, 497–517.

Johnson, J.W., Oeklers, E.H., Helgeson, H., 1992. SUPCRT92: a software package for calculating the standard molal thermodynamic properties of minerals, gases, aqueous species, and reactions for 1–5000 bar and 0–1000 °C. *Comput. Geosci.* **18**, 899–947.

JNC 1999. Project to Establish the Scientific and Technical Basis for HLW Disposal in Japan. Report H12, Japan Nuclear Cycle Development Institute, JNC, Tokai, Japan.

Kamei, G., Oda, C., Mitsui, S., Shibata, M., Shinozaki, T., 1999. Fe(II)–Na ion-exchange at interlayers of smectite: adsorption–desorption experiments and a natural analogue. *Eng. Geol.* **54**, 15–20.

Kodama, H., De Kimpe, C.R., Dejou, J., 1988. Ferroan saponite in a gabbro saprolite at Mont Blanc Magantic, Quebec. *Clays Clay Miner.* **36**, 102–110.

Kohyama, N., Shimoda, S., Sudo, T., 1973. Iron-rich saponite, ferric and ferrous forms. *Clays Clay Miner.* **21**, 229–237.

Lear, P.R., Stucki, J.W., 1989. Effects of iron oxidation –state on the specific surface area of nontronite. *Clays Clay Miner.* **37**, 547–552.

Lippman, F., 1977. The solubility products of complex minerals, mixed crystals and three layer clay minerals. *Neues Jahrb. Miner. Abh.* **130**, 243–263.

Lippman, F. 1982. The thermodynamic status of clay minerals. Proceedings of the Seventh International Clay Conference 1981, 475–485.

Madsen, F.T., 1998. Clay mineralogical investigations related to nuclear waste disposal. *Clay Miner.* **33**, 109–129.

Maier, C.G., Kelley, K.K., 1932. An equation for the representation of high temperature heat content data. *Am. Chem. Soc. J.* **54**, 3243–3246.

Manceau, A., Lanson, B., Drits, V.A., Chateigner, D., Gates, W.P., Wu, J., Huo, D., Stucki, J.W., 2000a. Oxidation–reduction mechanism of iron in dioctahedral 1. Crystal chemistry of oxidised reference nontronites. *Am. Mineral.* **85**, 133–152.

Manceau, A., Lanson, B., Drits, V.A., Chateigner, D., Gates, W.P., Wu, J., Huo, D., Stucki, J.W., 2000b. Oxidation–reduction mechanism of iron in dioctahedral smectites, 2. Crystal chemistry of reduced Garfield nontronite. *Am. Mineral.* **85**, 153–172.

Mattigod, S.V., Sposito, G., 1978. Improved method for estimating the standard free energies of formation, $\Delta G_{f,\ 298.15}$. of smectites. *Geochim. Cosmochim. Acta* **42**, 1753–1762.

May, H.M., Kinniburgh, D.G., Helmke, P.A., Jackson, M.L., 1986. Aqueous dissolution, solubilities and thermodynamic status of common alumnosilicate clay-minerals—kaolinites and smectites. *Geochim. Cosmochim. Acta* **50**, 1667–1677.

Mellini, M., Zanazzi, P.F., 1987. Crystal structures of lizardite-1T and lizardite-2H1 from Coli, Italy. *Am. Mineral.* **72**, 943–948.

Mercury, L., Vieillard, P., Tardy, Y., 2001. Thermodynamics of ice polymorphs and "ice-like" water in hydrates and hydroxides. *Appl. Geochem.* **16**, 161–181.

Merriman, R.J., Peacor, D.R., 1999. Very low grade metapelites, mineralogy, microfabrics and measuring reaction progress. In: Frey, M., Robinson, D. (Eds.), *Low Temperature Metamorphism*. Blackwell.

Meunier, A., Velde, B., Griffault, L., 1998. The reactivity of bentonites, a review. An application to clay barrier stability for nuclear waste storage. *Clay Miner.* **33**, 187–196.

Newman, A.C.D., Brown, G., 1987. The chemical constitution of clays. In: Newman, A.C.D. (Ed.), *Chem. Clay Clay Miner*. Wiley, New York.

Nriagu, J., 1975. Thermochemical approximations for clay minerals. *Am. Mineral.* **60**, 834–839.

Odin, G.S., 1988. *Green marine clays: oolitic ironstone facies, verdine facies, glaucony facies and celadonite-bearing facies: a comparative study. Developments in Sedimentology 45*. Elsevier, Oxford.

Oscarson, D.W., Dixon, D.A., Hume, D.B., 1996. Mass transport through defected bentonite plugs. *Appl. Clay Sci.* **11**, 127–142.

Pokrovskii, V.A., Helgeson, H.C., 1995. Thermodynamic properties of aqueous species and the solubilities of minerals at high pressures and temperatures: the system Al_2O_3–H_2O–HCl. *Am. J. Sci.* **295**, 1255–1342.

Pusch, R., 1992. Use of bentonite for isolation of radioactive waste products. *Clay Miner.* **27**, 353–361.

Pusch, R. 1993. Evolution of models for conversion of smectite to non-expandable minerals. SKB technical report TR-93-99. Swedish Nuclear Fuel and Waste Management Company Ltd. Stockholm, Sweden.

Ragnarsdottir, K.V., Walther, J.V., Arnorsson, S., 1984. Description and interpretation of the composition of fluid and alteration mineralogy in the geothermal system, at Svartsengi, Iceland. *Geochim. Cosmochim. Acta* **48**, 1535–1553.

Ransom, B., Helgeson, H.C., 1994a. A chemical and thermodynamic model of aluminous dioctahedral 2, 1 layer clay minerals in diagenetic processes, regular solution representation of interlayer dehydration in smectite. *Am. J. Sci.* **294**, 449–484.

Ransom, B., Helgeson, H., 1994b. Estimation of standard molal heat capacities, entropies, and volumes of 2:1 clay minerals. *Geochim. Cosmochim. Acta* **58**, 4537–4547.

Ransom, B., Helgeson, H.C., 1995. A chemical and thermodynamic model of dioctahedral 2, 1 layer clay and minerals in diagenetic processes, dehydration of smectite as a function of temperature and depth in sedimentary basins. *Am. J. Sci.* **295**, 245–281.

Refait, P., Memet, J.B., Bon, C., Sabot, R., Genin, J.M.R., 2003a. Formation of the Fe,II–Fe,III·hydroxysulphate green rust during marine corrosion. *Corros. Sci.* **45**, 833–845.

Refait, P., Benali, O., Abdelmoula, M., Genin, J.M.R., 2003b. Formation of "ferric green rust" and/or ferrihydrite by fast oxidation of iron, II–III·hydroxychloride green rust. *Corros. Sci.* **45**, 2435–2449.

Robinson, D., Bevins, R.E., Rowbotham, G., 1993. The characterisation of mafic phyllosilicates in low-grade metabasalts from eastern Greenland. *Am. Mineral.* **78**, 377–390.

Robinson, D., Schmidt, S.T., de Zamora, A.S., 2002. Reaction pathways and reaction progress for the smectite-to-chlorite transition: evidence from hydrothermally altered metabasites. *J. Metamorph. Geol.* **20**, 167–174.

Saccocia, P.J., Seyfried, W.E., 1993. A resolution of discrepant thermodynamic properties for chamosite retrieved from experimental and empirical techniques. *Am. Mineral.* **78**, 607–611.

Schiffman, P., Fridleiffson, G.O., 1991. The smectite–chlorite transition in drillhole NJ-15, Nesjavellir geothermal field, Iceland, XRD, BSE and electron microprobe investigations. *J. Metamorph. Geol.* **9**, 679–696.

Schiffman, P., Staudigel, H., 1995. The smectite to chlorite transition in a fossil seamount hydrothermal system, the basement complex of La Palma, Canary Islands. *J. Metamorph. Geol.* **13**, 487–498.

Schmidt, S.T., Robinson, D., 1997. Metamorphic grade and porosity and permeability controls on mafic phyllosilicate distributions in a regional zeolite to greenschist facies transition of the North Shore Volcanic Group, Minnesota. *Geol. Soc. Am. Bull.* **109**, 683–697.

Schwertmann, U., Murad, E., 1983. Effect of pH on the formation of goethite and hematite from ferrihydrite. *Clays Clay Miner.* **31**, 277–284.

Schwertmann, U., Fechter, H., 1994. The formation of green rust and its transformation to lepidocrocite. *Clay Miner.* **29**, 87–92.

Shau, Y.-H., Peacor, D.R., 1992. Phyllosilicates in hydrothermally altered basalts from DSDP Hole 504B, Leg 83-a TEM and AEM study. *Contrib. Miner. Petr.* **112**, 119–133.

Sherman, G.D., Ikawa, H., Uehara, G., Okazaki, E., 1962. Types of occurrence of nontronite and nontronite-like minerals in soils. *Pac. Sci.* **16**, 57–62.

Shock, E.L., Helgeson, H.C, 1988. Calculation of the thermodynamic and transport properties of aqueous species at high pressures and temperatures: correlation for ionic species and equation of state predictions to 5 kb and 1000 °C. *Geochim. Cosmochim. Acta* **52**, 2009–2036.

Shock, E.L., Helgeson, H.C., Sverjensky, D.A., 1989. Calculation of the thermodynamic and transport properties of aqueous species at high pressures and temperatures: standard partial molal properties of inorganic neutral species. *Geochim. Cosmochim. Acta* **53**, 2157–2183.

Siehl, A., Thein, J., 1989. Minette-type ironstones. In: Young, T.P., Taylor, W.E.H. (Eds.), *Phanerozoic Ironstones*, 46. Geological Society Special Publication, pp. 175–193.

Środoń, J., 1999. Nature of the mixed-layer clays and mechanisms of their formation and alteration. *Ann. Rev. Earth Planet. Sci.* **27**, 19–53.

Stucki, J.W., Roth, C.B., 1977. Oxidation–reduction mechanism for structural iron in nontronite. *Soil Sci. Soc. Am. J.* **41**, 808–814.

Stucki, J.W., Golden, D.C., Roth, C.B., 1984. Effects of reduction and reoxidation of structural iron on the surface charge and dissolution of dioctahedral smectites. *Clays Clay Miner.* **32**, 350–356.

Stucki, J.W., Tessier, D., 1991. Effect of iron oxidation state on the texture and structural order of Na-montmorillonite gels. *Clays Clay Miner.* **39**, 137–143.

Stucki, J.W., Bailey, G.W., Gan, H., 1996. Oxidation–reduction mechanisms in iron-bearing phyllosilicates. *Appl. Clay Sci.* **10**, 417–430.

Tamaura, Y., Yoshida, T., Katsura, T., 1984. The synthesis of green rust II, FeIII1–FeII2 and its spontaneous transformation to Fe_3O_4. *Bull. Chem. Soc. Jpn* **57**, 2411–2416.

Tardy, Y., Garrels, R.M., 1974. A method of estimating the Gibbs energies of formation of layer silicates. *Geochim. Cosmochim. Acta* **38**, 1101–1116.

Tardy, Y., Fritz, B., 1981. An ideal solid solution model for calculating solubility of clay minerals. *Clay Miner.* **16**, 361–373.

Tardy, Y., Duplay, J., 1992. A new method of estimating the Gibbs free energy of formation of hydrated and dehydrated clay minerals. *Geochim. Cosmochim. Acta* **56**, 3007–3029.

Tardy, Y., Mercury, L., Roquin, C., Vieillard, P., 1999. The concept of ice-like water: hydration–dehydration of salts, hydroxides, clay minerals, and living or inert organic matter. *Comptes Rendus de L'Academie des Sciences Serie II Fascicule A-Sciences de La Terre et des Planetes* **329**, 377–388.

Taylor, K.G., 1990. Berthierine from the non-marine Wealden, Early Cretaceous sediments of the South-East England. *Clay Miner.* **25**, 391–399.

Toth, T.A., Fritz, S.J., 1997a. An Fe-berthierine from a Cretaceous laterite 1. Characterization. *Clays Clay Miner.* **45**, 564–579.

Toth, T.A., Fritz, S.J., 1997b. An Fe-berthierine from a Cretaceous laterite 2. Estimation of Eh, pH and pCO_2conditions of formation. *Clays Clay Miner.* **45**, 580–586.

Van Houten, F.B., Purucker, M.E., 1984. Glauconitic peloids and chamositic ooids—favourable factors, constraints, and problems. *Earth Sci. Rev.* **20**, 211–243.

Vieillard, P., 2000. A new method for the prediction of Gibbs free energies of formation of hydrated clay minerals based on the electronegativity scale. *Clays Clay Miner.* **48**, 459–473.

Vieillard, P., 2002. A new method for the prediction of Gibbs free energies of phylosilicates, 10 angstroms and 14 angstroms based on the electronegativity scale. *Clays Clay Miner.* **50**, 352–363.

Wanner, H., Albinsson, Y., Karnland, O., Wieland, E., Wersin, P., Charlet, L., 1994. The acid/base chemistry of montmorillonite. *Radiochim. Acta* **66/77**, 157–162.

Wolery, T. 1979. Calculation of equilibrium between aqueous solution and minerals: the EQ3/6 software package: Lawrence Livermore National Laboratory, UCRL-52658.

Wolery, T., 1996. *EQ3/6 Database*. Lawrence Livermore National Laboratory, USA.

Wilson, J., Cuadros, J., Cressey, G., 2004. An in situ time-resolved XRD–PSD investigation into Na-montmorillonite interlayer and particle rearrangement during dehydration. *Clays Clay Miner.* **52**, 180–191.

Wilson, J., Cressey, G., Cressey, B., Cuadros, J., Ragnarsdottir, K.V., Savage, D., Shibata, M., 2006. The effect of iron on montmorillonite stability. (II) Experimental investigation. *Geochim. Cosmochim. Acta* **70**, 323–336.

Wu, T.-C., Bassett, W.A., Huang, W.-L., Guggenheim, S., Koster van Groos, A.F., 1997. Montmorillonite under high H_2O pressures, stability of hydrate phases, rehydration hysteresis and the effect of interlayer cations. *Am. Mineral.* **82**, 69–78.

Zheng, H., Bailey, S.W., 1997. Refinement of an amesite-2H, sub1. polytype from Postmasburg, South Africa. *Clays Clay Miner.* **45**, 301–310.

View publication stats